



Atractylenolide II regulates the proliferation, ferroptosis, and immune escape of hepatocellular carcinoma cells by inactivating the TRAF6/NF- κ B pathway

Yujie Lin¹ · Ke Chen¹ · Min Zhu¹ · Wei Song² · Guiyun Wu³ · Aizhen Pan¹

Received: 5 January 2024 / Accepted: 9 March 2024

© The Author(s), under exclusive licence to Springer-Verlag GmbH Germany, part of Springer Nature 2024

Abstract

Hepatocellular carcinoma (HCC) is a common and lethal tumor worldwide. Atractylenolide II (AT-II) is a natural sesquiterpenoid monomer, with anti-tumor effect. To address the effect and mechanisms of AT-II on HCC. The role and mechanisms of AT-II were assessed through cell counting kit-8, flow cytometry, enzyme-linked immunosorbent assay, immunofluorescence, and western blot experiments in Hep3B and Huh7 cells. *In vivo* experiments were conducted in BALB/c nude mice using immunohistochemistry and western blot assays. AT-II decreased the cell viability of Hep3B and Huh7 cells with a IC50 of 96.43 μ M and 118.38 μ M, respectively. AT-II increased relative Fe²⁺ level, which was further promoted with the incubation of erastin and declined with the ferrostatin-1 in Hep3B and Huh7 cells. AT-II enhanced the level of ROS and MDA, but reduced the GSH level, and the expression of xCT and GPX4. AT-II elevated the percent of CD8+ T cells and the IFN- γ contents, and declined the IL-10 concentrations and the expression of PD-L1 in Hep3B and Huh7 cells. AT-II downregulated the relative protein level of TRAF6, p-p65/p-65, and p-I κ B α /I κ B α , which was rescued with overexpression of TRAF6. Upregulation of TRAF6 also reversed the effect of AT-II on proliferation, ferroptosis, and immune escape in Hep3B cells. *In vivo*, AT-II reduced tumor volume and weight, the level of GPX4, xCT, and PD-L1, and the expression of TRAF6, p-p65/p-65, and p-I κ B α /I κ B α , with the increased expression of CD8. AT-II modulated the proliferation, ferroptosis, and immune escape of HCC cells by downregulating the TRAF6/NF- κ B pathway.

Keywords Hepatoma · Atractylenolide II · Ferroptosis · Immune escape · TRAF6 · NF- κ B

Yujie Lin and Ke Chen contributed equally to this work.

✉ Guiyun Wu
jabnamk@163.com

✉ Aizhen Pan
panaizhenpaz@21cn.com

¹ Department of Traditional Chinese Medicine, Sun Yat-sen Memorial Hospital Affiliated to Sun Yat-sen University, Yuexiu District, No. 107, Yanjiang West Road, Guangzhou Guangdong Province 510120, China

² Department of Gastroenterology, Sun Yat-sen Memorial Hospital Affiliated to Sun Yat-sen University Shenshan Central Hospital, Shanwei 516600, China

³ Department of Anesthesiology, Sun Yat-sen Memorial Hospital Affiliated to Sun Yat-sen University, Yuexiu District, No. 107, Yanjiang West Road, Guangzhou Guangdong Province 510120, China

Introduction

Hepatocellular carcinoma (HCC) is the sixth most frequent tumor and the fourth biggest cause of tumor-related mortality around the world (Konyn et al. 2021; Vogel et al. 2022). It is estimated that one million populations will suffer HCC by 2025 worldwide with Chinese suffering accounting for about 53% (Bray et al. 2018). The etiology and pathogenesis of HCC are tanglesome, which have not been totally clarified at present. Yet, some sharing hallmarks of malignancies, such as aberrant proliferation, immune evasion, and activating invasion and metastasis, have been identified to be strongly related to the progression and development of HCC (Hanahan 2022). Locoregional therapy, containing liver transplantation, radiofrequency ablation, and surgical resection, is an effective approach for the treatment of HCC diagnosed at an early stage (Galle et al. 2021; Zhou and Song 2021). However, owing to the shortage of early diagnosis, HCC is generally found at an advanced stage,

which makes locoregional therapy feeble (Sugawara and Hibi 2021). Although radiotherapy and chemotherapy are feasible for patients diagnosed at advanced stages, resistance as well as severe side effects have seriously impeded their clinical application (Nia and Dhanasekaran 2020; Chen et al. 2021). Consequently, the fact of high incidence of metastasis and recurrence contributes to low overall 5-year survival rate of HCC under 20% (Kishore et al. 2020). Therefore, dissecting the potential molecular mechanisms of HCC to develop viable therapies is of prime importance for the treatment of HCC.

Atractylenolide, a sesquiterpene, is one of the principal components of *Atractylodes macrocephala* that has various pharmacological properties (Xie et al. 2023). Atractylenolides comprise atractylenolide I, II, and III, and all these three components exhibit potent anti-tumor activities in different tumors, such as colon cancer, gastric cancer, and lung cancer (Xie et al. 2023). Sheng and colleagues (Sheng et al. 2021) have reported that atractylenolide III effectively inhibits HCC cell growth and evokes cell apoptosis by upregulating miR-195-5p to downregulate FGFR1 expression. The object of this study, atractylenolide II (AT-II), has exhibited a suppressive effect on inflammation, oxidative stress, and radiation based on plenty of studies (Li et al. 2007; Li et al. 2007; Wang et al. 2011; Xiao et al. 2020). Besides, AT-II exerts gastroprotective activity to prevent gastric ulcer induced by ethanol both *in vivo* and *in vitro* (Wang et al. 2010). Moreover, the anti-tumor effect of AT-II has been identified on different tumors. For instance, the encouraging effect of AT-II on cell cycle arrest and apoptosis by the androgen receptors (ER) pathway has been reported in breast cancer (Dou et al. 2021). AT-II dampens cell viability and ameliorates chemoresistance in colorectal cancer (Zhang et al. 2019). AT-II suppresses cell proliferation and enhances G2/M cell cycle arrest-induced apoptosis in prostate cancer (Wang et al. 2018). Nevertheless, the function and possible mechanisms of AT-II in HCC still need to be addressed further.

Therefore, the effect and possible mechanisms of AT-II were explored in HCC cell lines and xenografted mice. We hope our results can identify an efficient agent for the treatment of HCC.

Materials and methods

Reagents

AT-II was bought from MedChemExpress (catalog number: HY-N0202, Monmouth Junction, NJ, USA) with a purity of 99.91%, dissolved in dimethylsulfoxide (DMSO, catalog number: ST038, Beyotime), and then diluted in PBS for the use.

Cell culture

The normal hepatocyte line THLE-3 was bought from ATCC (catalog number: CRL-11233), and two HCC cell lines Hep3B (catalog number: CL-0120) and Huh7 (catalog number: CL-0120) were prepared from Procell (Wuhan, China). THLE-3 cells were grown in MEM (catalog number: 41500034, Gibco, Rockville, MD, USA), and Hep3B and Huh7 cells were grown in DMEM (catalog number: PM150210, Procell) with 10% fetal bovine serum (FBS, 12103C, Merck, Whitehouse Station, NJ, USA) and 1% penicillin/streptomycin (P/S, PB180120, Procell) in an incubator at 37 °C with 5% CO₂.

Cell treatments

AT-II with concentrations of 0, 12.5, 25, 50, 100, 200, and 400 μM was used to incubate with THLE-3 cells for 48 h to assess the toxic effect of AT-II on THLE-3 cells, and AT-II with the concentrations of 0, 12.5, 25, 50, 100, and 200 μM was used to incubate with Hep3B and Huh7 cells to assess the toxic effect of AT-II on Hep3B and Huh7 cells. The serial concentrations of AT-II used in the present were based on the previous studies (Wang et al. 2018; Tian and Yu 2017). 0 μM AT-II used in the present study indicated that cells were hatched with PBS (catalog number: ST447, Beyotime). Besides, 5 mmol/L erastin (an activator of ferroptosis) or 1 mmol/L ferrostatin-1 (an inhibitor of ferroptosis) was used to incubate with Hep3B and Huh7 cells to determine the direct role of ferroptosis. The concentration of erastin and ferrostatin-1 used in the present study was according to the report (Zhang et al. 2021). In addition, the sequences of tumor necrosis factor receptor-associated factor 6 (TRAF6) were interposed into pcDNA vector plasmids, which were transfected into Huh7 cells to enhance the level of TRAF6 by Lipofectamine 3000 (catalog number: L3000001, Invitrogen, Carlsbad, CA, USA). Cells were yielded for the subsequent experiments after 48 h of transfection.

Cell counting kit-8 (CCK-8) assay

THLE-3, Hep3B, and Huh7 cells with 1×10^4 cells/well were filled into 96-well plates and grown at 37 °C with 5% CO₂. The cell viability was evaluated by a cell counting kit-8 kit (catalog number: C0037, Beyotime, Shanghai, China) by appending 10 μl CCK-8 reagent into each well for treatment for 2 h at 37 °C. The absorbance at 450 nm was recorded with a microplate reader (Thermo Fisher Scientific, Waltham, MA, USA).

Detection of the ferrous iron level

Two HCC cell lines were collected and centrifuged at 300 g for 10 min at 4 °C. After removing the supernatant, cells were subjected to ultrasonication and then centrifuged at 15,000 g for 10 min at 4 °C to collect the supernatant for detection. The level of ferrous iron of two HCC cell lines was examined by an Iron Assay Kit (catalog number: ab83366, Abcam, Cambridge, UK) in keeping with the working instructions.

Examination of the ROS level

The relative fluorescence intensities were measured by a fluorescence microscope (catalog number: IX71, Olympus, Tokyo, Japan) after two HCC cell lines were treated with 2 μM 5-(and-6)-chloromethyl-2-,7-dichlorofluorescein diacetate (DCFH-DA, catalog number: S0033S, Beyotime) at 37 °C for half an hour without light.

Detection of the MDA and GSH level

The contents of glutathione (GSH) and malondialdehyde (MDA) in HCC cell lines were examined using the Reduced Glutathione (GSH) Content Assay Kit (catalog number: D799613, Sangon Biotech, Shanghai, China) and Malondialdehyde (MDA) Content Assay Kit (catalog number: D799761, Sangon Biotech) based on the working instructions.

Flow cytometry assay

The main cell types of PBMCs are cells with a single nucleus in the blood, including lymphocytes (T cells, B cells, and NK cells), monocytes, phagocytic cells, dendritic cells, and a few other cell types. The immune system's role in protecting the body against tumors is crucial, and a key component of this anti-tumor response lies in the ability of certain immune cells, such as cytotoxic T cells and natural killer cells, to induce malignant cell death through the immune cell killing (ICK) process. Thus, to assess the role of AT-II in the immune escape, PBMCs were separated from whole blood using Human Peripheral Blood Lymphocyte Separation Medium (catalog number: C0025, Beyotime) based on the working instructions. Subsequently, two HCC cells with cell density of 2.5×10^5 /well (mL) were co-cultured with PBMC density of 2.5×10^5 cells/well (mL) in the presence of AT-II (50, 100, and 200 μM) and incubated for 48 h. The suspending PBMC cells were collected for flow cytometric analysis on a FACScan flow cytometry (Thermo Fisher Scientific) after incubated with CD3 (catalog number: 14-0037-82, Invitrogen) and CD8 (catalog number: 12-0088-42, Invitrogen) antibody on ice for half an hour without light.

Enzyme-linked immunosorbent assay (ELISA)

The contents of interferon-γ (IFN-γ) and interleukin-10 (IL-10) in the media of co-culture cells were measured with Human IFN-γ ELISA Kit (catalog number: PI511, Beyotime) and Human IL-10 ELISA Kit (catalog number: PI528, Beyotime) in keeping with the working manuals. The absorbance was recorded at 450 nm by a microplate reader (Thermo Fisher Scientific).

Immunofluorescence (IF) assay

Two HCC cell lines were seeded on glassy plates and grown in an incubator with 5% CO₂ at 37 °C overnight. After the treatments, cells were rinsed with PBS three times, immobilized with 4% paraformaldehyde (catalog number: P0099, Beyotime) at room temperature for 15 min, rinsed with PBS thrice, permeabilized with 0.5% Triton X-100 (catalog number: P0096, Beyotime) at room temperature for 20 min, and rinsed with PBS for three times. Next, cells were treated with the antibodies targeted to p65 (1:500, catalog number: ab16502, Abcam) at 4 °C overnight and Goat anti-rabbit IgG-AlexaFluor 488 (1:1000, catalog number: ab150077, Abcam) at 37 °C for 1 h, respectively. Then, cells were mounted with Mounting Medium, anti-fading (with DAPI) (catalog number: P0131, Beyotime), and imaged with fluorescence microscopy.

Animal

All animal experiments were kept with the Animal Research Ethics Committee of our hospital (approval number: SYSKY-2022-225-02). BALB/c nude mice (4 weeks old) were bought from Cyagen (Jiangsu, China). Mice were bred in a specified pathogen-free (SPF) condition with a 12-h cycle of light-dark at 22–24 °C, and provided with water and rodent diets *ad asbitsium*. Mice were subcutaneously inoculated with 1×10^6 of Huh7 cells (Cai et al. 2021), and then stochastically allotted into sham group and AT-II 50 mg/kg group with five mice in each group. Mice in the AT-II 50 mg/kg group and sham group were intragastrically administrated with 50 mg/kg AT-II and PBS, severally. The dose of AT-II used in the present study was following the previous study (Zhang et al. 2022). Mouse body weight and tumor volume were examined every 1 week for successive 4 weeks. Tumor volume was determined with the following formula: volume = $1/2 \times \text{length} \times \text{width}^2$ (Cardenas et al. 2009). Mice were sacrificed by inhaling the excess isoflurane (R510-22, RWD, Guangdong, China), and tumor samples were excised, weighed, and stored for subsequent assays.

Immunohistochemistry (IHC) assay

Tumor tissues were excised and soaked into 4% paraformaldehyde, and then dehydrated with gradient concentrations of ethanol. Next, the tissues were encapsulated into paraffin (catalog number: YA0011, Solarbio, Beijing, China) and then sectioned into slices with a thickness of 5 μm . Subsequently, slices were subjected to drying, deparaffinization, and restoration with the Citrate Antigen Retrieval Solution (pH 6.0, catalog number: P0081, Beyotime) for 15 min at 94 $^{\circ}\text{C}$. After the block with 1% BSA (catalog number: ST2249, Beyotime) for 30 min, slices were treated with the primary antibodies against glutathione peroxidase 4 (GPX4) (catalog number: ab125066, 1:250, Abcam), cystine/glutamic acid transporter (xCT) (catalog number: ab307601, 1:500, Abcam), programmed death-ligand 1 (PD-L1) (catalog number: ab233482, 1:100, Abcam) and CD8 (catalog number: PA5-88265, 1:200, Invitrogen), and the secondary antibody labeled with HRP (catalog number: ab6721, 1:1000, Abcam). Finally, slices were re-dyed with hematoxylin (catalog number: C0107, Beyotime) and imaged under a light microscope (Olympus).

Western blot

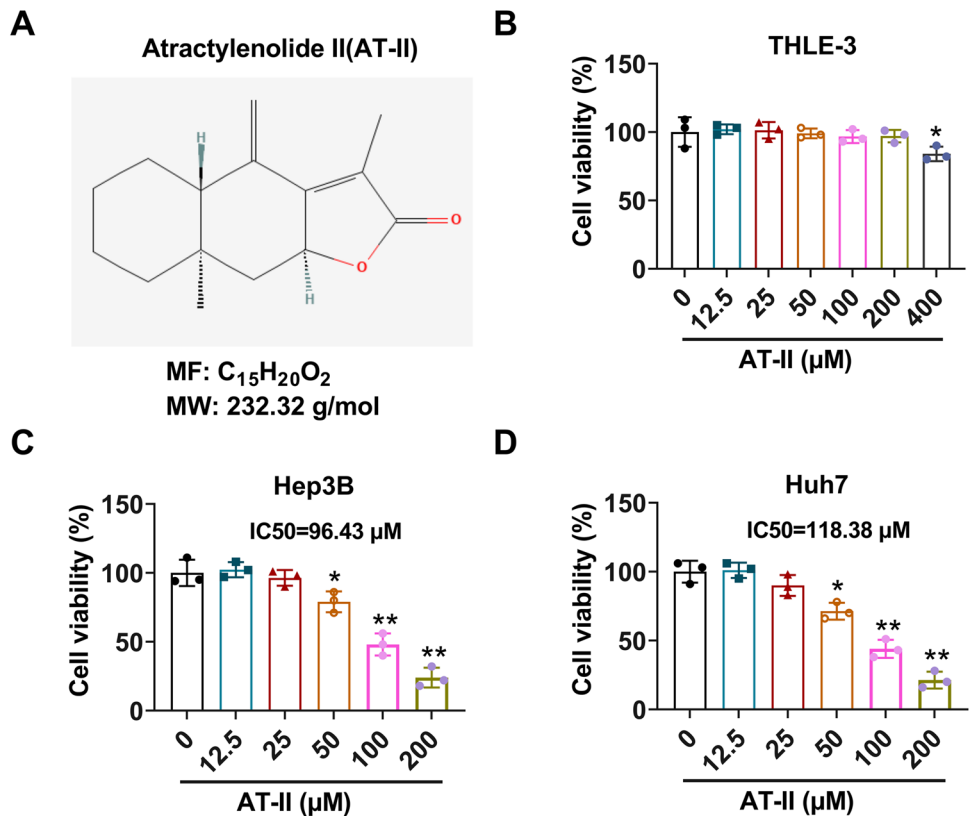
Total protein was collected from HCC cell lines and tumor tissues by the RIPA Lysis Buffer (catalog number: P0013K,

Beyotime), and quantified with the BCA Protein Assay Kit (catalog number: P0010, Beyotime). Protein samples measuring 20 μg were subjected to 10% sodium dodecyl sulfate polyacrylamide gel electrophoresis (SDS-PAGE) and shifted onto PVDF membranes (catalog number: HVHP04700, Millipore, Billerica, MA, USA). The membranes were sealed with Blocking Buffer (catalog number: P0023B, Beyotime), and treated with primary antibodies at 4 $^{\circ}\text{C}$ overnight. The membranes were hatched with goat anti-rabbit IgG H&L (HRP) (catalog number: ab6721, 1:10000, Abcam) at 37 $^{\circ}\text{C}$ for 1 h. The membranes were developed with the BeyoECL Plus (catalog number: P0018S, Beyotime) before the band intensity was determined by QUANTITY ONE software (Bio-Rad, Hercules, CA, USA). The primary antibodies contained anti-GPX4 (catalog number: ab125066, 1:10000, Abcam), anti-xCT (catalog number: ab307601, 1:1000, Abcam), anti-PD-L1 (catalog number: ab233482, 1:1000, Abcam), anti-TRAF6 (catalog number: ab137452, 1:3000, Abcam), anti-p65 (catalog number: ab16502, 1:1000, Abcam), anti-p-p65 (catalog number: ab86299, 1:10000, Abcam), anti-IkB α (catalog number: ab97783, 1:10000, Abcam), anti-p-IkB α (catalog number: ab133462, 1:10000, Abcam), and anti- β -actin (catalog number: ab5694, 1:1000, Abcam).

Statistical analysis

Data were presented as mean \pm standard deviation (SD). Difference was tested by the Student's *t*-test (for two groups)

Fig. 1 AT-II repressed the proliferation of Hep3B and Huh7 cells. **A** The 2-dimensional structure of AT-II. **B** The cell viability of THLE-3 cells treated with 0, 12.5, 25, 50, 100, 200, and 400 μM AT-II for 48 h was examined by CCK-8 assays. **C** The cell viability of Hep3B cells treated with 0, 12.5, 25, 50, 100, and 200 μM AT-II for 48 h was examined by CCK-8 assays. **D** The cell viability of Huh7 cells treated with 0, 12.5, 25, 50, 100, and 200 μM AT-II for 48 h was examined by CCK-8 assays. **P* < 0.05 and ***P* < 0.01 vs. 0 μM AT-II. *n* = 3



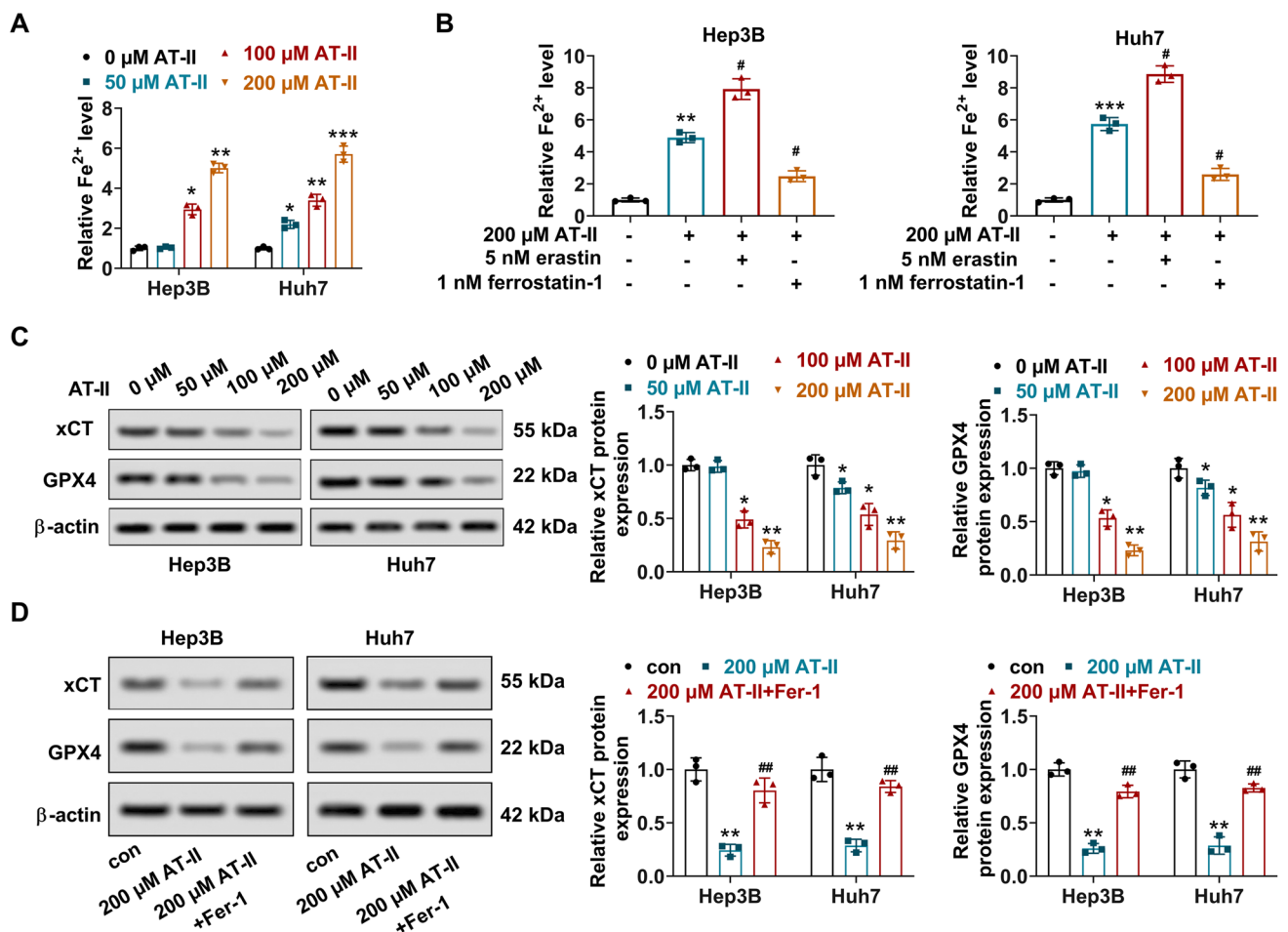


Fig. 2 The effect of AT-II on the Fe²⁺ level and the expression of xCT and GPX4 in Hep3B and Huh7 cells. **A** The relative Fe²⁺ level was detected after Hep3B and Huh7 cells were treated with 50, 100, and 200 μM AT-II for 48 h. **P* < 0.05, ***P* < 0.01, and ****P* < 0.001 vs. 0 μM AT-II. **B** The relative Fe²⁺ level was detected after Hep3B and Huh7 cells were treated with 200 μM AT-II accompanied with erastin or ferrostatin-1. ***P* < 0.01 and ****P* < 0.001 vs. control (without 200 μM AT-II, erastin and ferrostatin-1); #*P* < 0.05 vs. 200 μM AT-II. **C** The relative protein expression of xCT and GPX4 was

examined by western blot after Hep3B and Huh7 cells were treated with 50, 100, and 200 μM AT-II for 48 h. Data were expressed after being normalized with β-actin. **P* < 0.05 and ***P* < 0.01 vs. 0 μM AT-II. **D** The relative protein expression of xCT and GPX4 was determined by western blot after Hep3B and Huh7 cells were treated with 200 μM AT-II accompanied with ferrostatin-1. Data were expressed after being normalized with β-actin. ***P* < 0.01 vs. con; ##*P* < 0.01 vs. 200 μM AT-II. *n* = 3

or the one-way analysis of variance (ANOVA) (for more than two groups) followed by *post hoc* Bonferroni test by the SPSS 22.0 statistical software (IBM, Armonk, New York, USA). *P* < 0.05 was defined as a significant difference.

Results

AT-II suppressed the proliferation of HCC cells

To survey the effect of AT-II on HCC, AT-II (Fig. 1A) with concentrations of 0, 12.5, 25, 50, 100, and 200 μM was used to incubate with Hep3B and Huh7 cells for 48 h. AT-II ranged from 12.5 to 200 μM had no influence on the cell viability

of the normal hepatocyte line THLE-3, while the THLE-3 cell viability was markedly reduced with the incubation of 400 μM (Fig. 1B). On the other hand, AT-II with the concentrations of 50, 100, and 200 μM significantly declined the cell viability of both Hep3B and Huh7 cells, with a IC₅₀ of 96.43 μM and 118.38 μM, respectively (Fig. 1C and D), thus these three concentrations of AT-II (50, 100, and 200 μM) were chosen for the following studies. Totally, these results indicated that AT-II repressed the proliferation of HCC cells.

AT-II enhanced ferroptosis in HCC cells

To address the effect of AT-II on ferroptosis in HCC cells, Hep3B and Huh7 cells were incubated with 50, 100, and

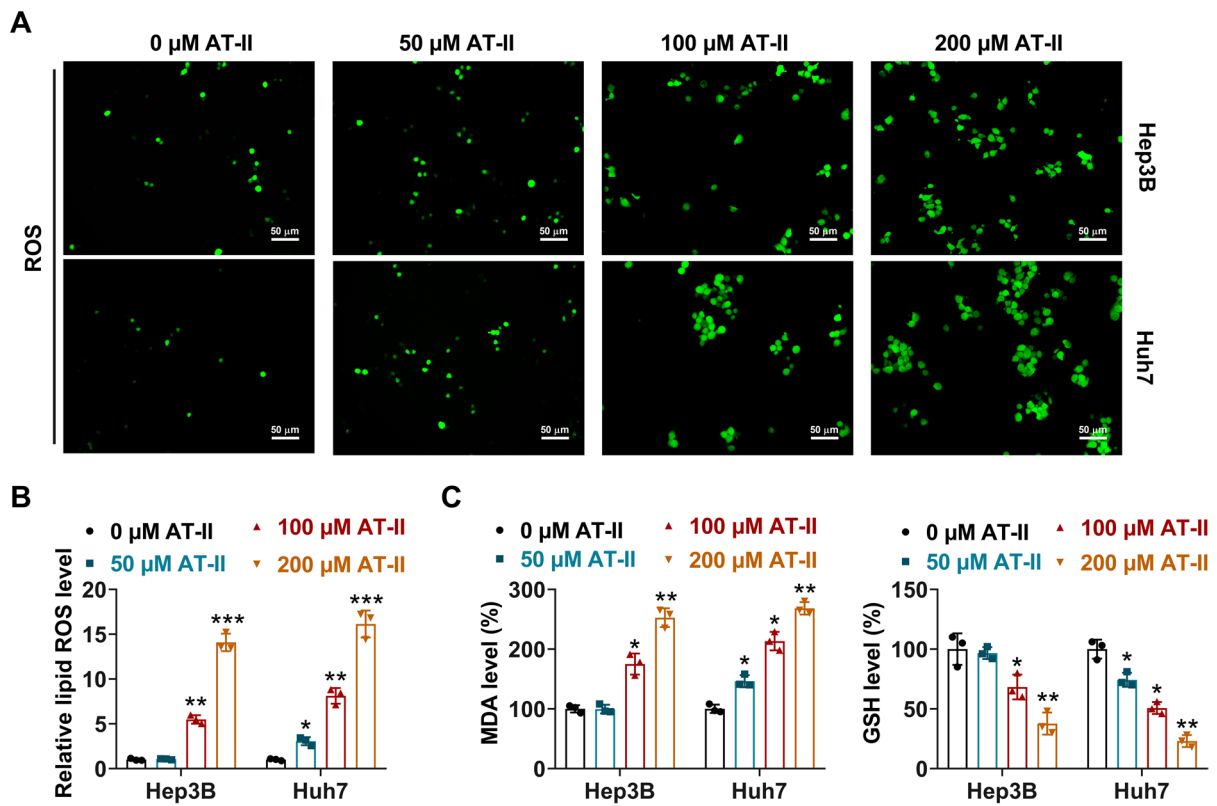


Fig. 3 Effect of AT-II on the level of ROS, MDA, and GSH in Hep3B and Huh7 cells. **A** and **B** The relative lipid ROS level was examined after Hep3B and Huh7 cells were incubated with 50, 100, and 200 μM AT-II for 48 h. **C** The relative lipid MDA and GSH levels were

detected after Hep3B and Huh7 cells were incubated with 50, 100, and 200 μM AT-II for 48 h. * $P < 0.05$, ** $P < 0.01$, and *** $P < 0.001$ vs. 0 μM AT-II. $n = 3$

200 μM AT-II for 48 h. The relative Fe^{2+} level was notably increased after Hep3B cells were treated with 100 and 200 μM AT-II, and that was markedly elevated after Huh7 cells were hatched with 50, 100, and 200 μM AT-II (Fig. 2A). To further confirm the direct role of ferroptosis, erastin and ferrostatin-1 were used to incubate with Hep3B and Huh7 cells. Treatment of AT-II causing the increased relative Fe^{2+} level was prominently further promoted with the incubation of erastin, but notably declined with the introduction of ferrostatin-1 in Hep3B and Huh7 cells (Fig. 2B). Besides, the relative protein expression of xCT and GPX4 was markedly decreased in Hep3B cells treated with 100 and 200 μM AT-II [xCT: 0 μM (1 ± 0.05), 50 μM (0.99 ± 0.06), 100 μM (0.49 ± 0.08), 200 μM (0.23 ± 0.06); GPX4: 0 μM (1 ± 0.06), 50 μM (0.97 ± 0.06), 100 μM (0.53 ± 0.08), 200 μM (0.23 ± 0.05)], and in Huh7 cells administrated with 50, 100, and 200 μM AT-II [xCT: 0 μM (1 ± 0.10), 50 μM (0.79 ± 0.06), 100 μM (0.54 ± 0.10), 200 μM (0.29 ± 0.08); GPX4: 0 μM (1 ± 0.09), 50 μM (0.82 ± 0.07), 100 μM (0.56 ± 0.12), 200 μM (0.31 ± 0.09)] (Fig. 2C).

The reduced expression of xCT and GPX4 in AT-II-induced Hep3B and Huh7 cells was significantly restored with the treatment of ferrostatin-1 (Fig. 2D). Moreover, the relative lipid ROS level was prominently increased in Hep3B cells hatched with 100 and 200 μM AT-II, and in Huh7 cells administrated with 50, 100, and 200 μM AT-II (Fig. 3A and B). Treatment of 100 and 200 μM AT-II significantly enhanced the MDA level, but decreased the GSH level in Hep3B cells (Fig. 3C). Administration of 50, 100, and 200 μM AT-II markedly increased the MDA level, but reduced the GSH level in Huh7 cells (Fig. 3C). Altogether, these results suggested that AT-II promoted ferroptosis in Hep3B and Huh7 cells.

AT-II suppressed immune escape in HCC cells

In addition, the effect of AT-II on immune escape was resolved in Hep3B and Huh7 cells. As exhibited in Fig. 4A, the percent of CD8+ T cells was notably increased in Hep3B cells treated with 100 and 200 μM AT-II, and in Huh7 cells administrated with 50,

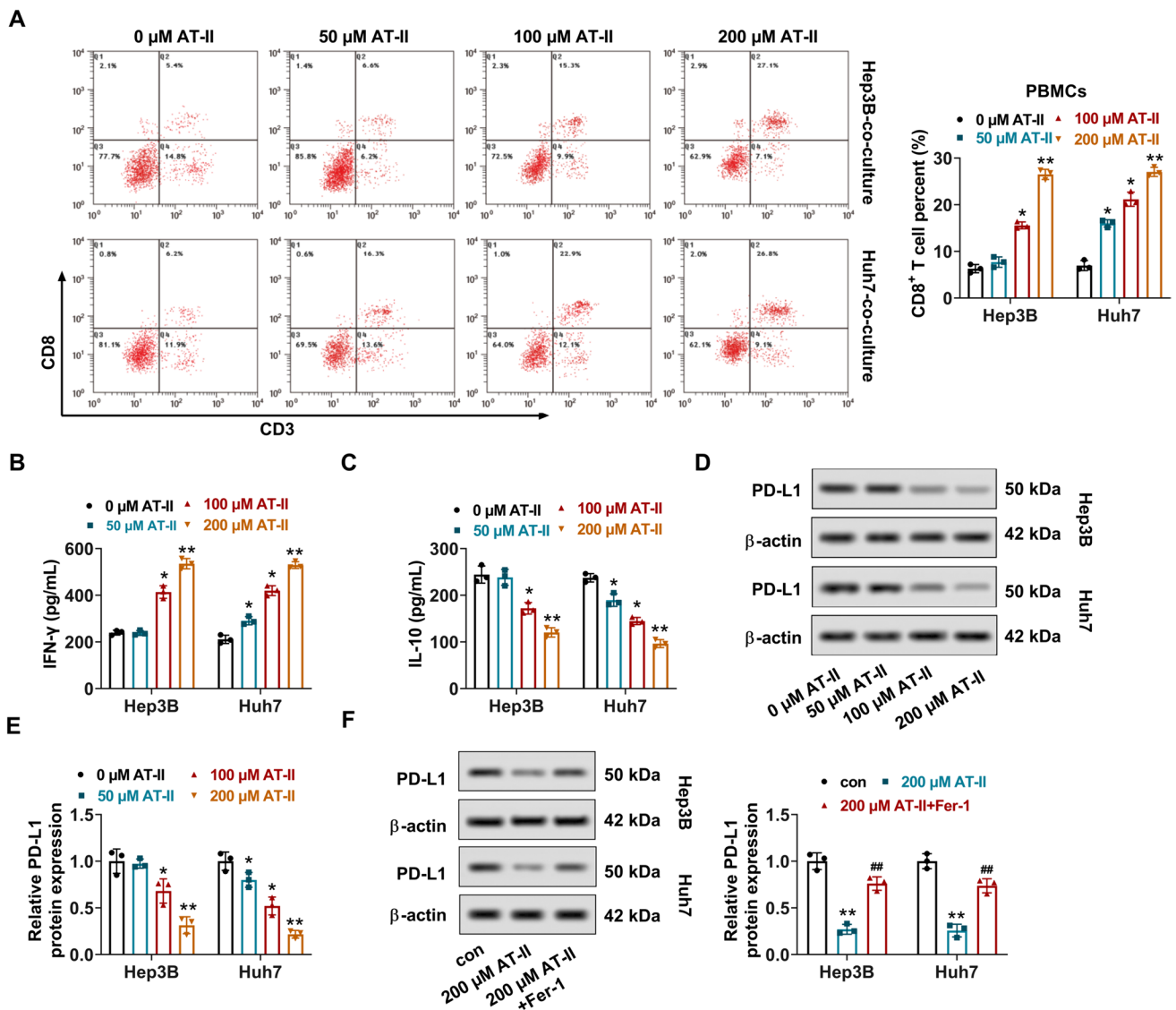


Fig. 4 AT-II repressed immune escape in Hep3B and Huh7 cells. Hep3B and Huh7 cells were incubated with 50, 100, and 200 μM AT-II for 48 h. **A** The percent of CD8⁺ T cells was detected by flow cytometry. **P* < 0.05, and ***P* < 0.01 vs. 0 μM AT-II. **B** The concentrations of IFN-γ were measured by ELISA. **P* < 0.05, and ***P* < 0.01 vs. 0 μM AT-II. **C** The concentrations of IL-10 were measured by ELISA. **P* < 0.05, and ***P* < 0.01 vs. 0 μM AT-II. **D** and **E** The

relative protein expression of PD-L1 was examined by western blot. Data were expressed after being normalized with β-actin. **P* < 0.05, and ***P* < 0.01 vs. 0 μM AT-II. **F** The relative protein expression of PD-L1 was examined by western blot after Hep3B and Huh7 cells were treated with 200 μM AT-II accompanied with ferrostatin-1. Data were expressed after being normalized with β-actin. ***P* < 0.01 vs. con; ###*P* < 0.01 vs. 200 μM AT-II. *n* = 3

100, and 200 μM AT-II. Moreover, similar results were found in the contents of IFN-γ (Fig. 4B), but reverse outcomes were discovered in the concentrations of IL-10 (Fig. 4C) in Hep3B and Huh7 cells. Furthermore, the relative protein expression of PD-L1 was markedly decreased in Hep3B cells treated with 100 and 200 μM AT-II, and in Huh7 cells administrated with 50, 100, and 200 μM AT-II (Fig. 4D and E). However, these reductions were prominently recovered with the administration

of ferrostatin-1 in Hep3B and Huh7 cells (Fig. 4F). Collectively, AT-II inhibited immune escape in Hep3B and Huh7 cells.

AT-II inhibited TRAF6/NF-κB pathway in HCC cells

To discover the possible mechanism of AT-II in HCC cells, the expression of TRAF6/NF-κB pathway was examined after Hep3B and Huh7 cells were hatched with 50, 100,

and 200 μM AT-II. The relative protein level of TRAF6, p-p65/p-65, and p-IkB α /IkB α was notably reduced in Hep3B cells administrated with 100 and 200 μM AT-II, and in Huh7 cells hatched with 50, 100, and 200 μM AT-II (Fig. 5A and B). Moreover, the nuclear level of p65 was obviously decreased after both Hep3B and Huh7 cells were treated with 200 μM AT-II (Fig. 5C). To further confirm the direct role of TRAF6/NF- κB pathway, TRAF6 was overexpressed in Huh7 cells (Fig. 6A). Overexpression of TRAF6 significantly restored AT-II-induced reduction in the relative protein level of TRAF6, p-p65/p-65, and p-IkB α /IkB α in Huh7 cells (Fig. 6B). Thus, AT-II down-regulated the expression of TRAF6/NF- κB pathway in Hep3B and Huh7 cells.

AT-II regulated the proliferation, ferroptosis, and immune escape of HCC cells by inactivating the TRAF6/NF- κB pathway

Moreover, overexpression of TRAF6 prominently rescued AT-II-induced decrease in the cell viability of Huh7 cells (Fig. 7A). Management of AT-II significantly increased the relative Fe $^{2+}$ level and ROS level in Huh7 cells, which

was observably offset with the overexpression of TRAF6 (Fig. 7B–D). Besides, a prominent elevation in the concentrations of IFN- γ resulting from the treatment of AT-II was significantly neutralized with the overexpression of TRAF6 in Huh7 cells (Fig. 7E). Furthermore, overexpression of TRAF6 prominently recovered AT-II-induced reduction in the contents of IL-10, as well as the relative protein level of PD-L1 in Huh7 cells (Fig. 7F and G). Overexpression of TRAF6 alone increased the cell viability, the IL-10 concentration, and the PD-L1 expression, but reduced the relative Fe $^{2+}$ level, the ROS level, and the concentrations of IFN- γ in Huh7 cells as compared with these in the control group (Fig. 7A–G). Therefore, these results indicated that AT-II modulated the proliferation, ferroptosis, and immune escape of Huh7 cells by inactivating the TRAF6/NF- κB pathway.

AT-II modulated the proliferation, ferroptosis, and immune escape involved in the downregulation of the TRAF6/NF- κB pathway *in vivo*

To verify the effect of AT-II *in vivo*, BALB/c nude mice were subcutaneously injected with 1×10^6 of Huh7 cells, and the

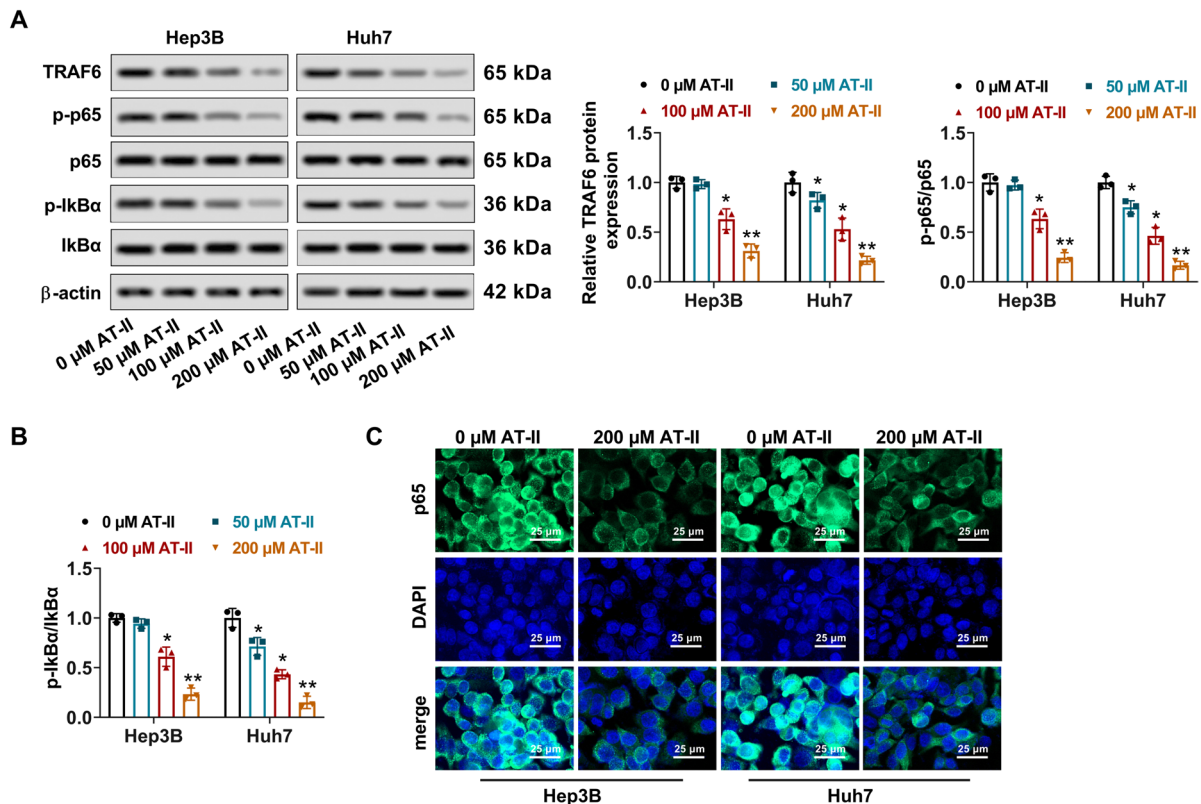
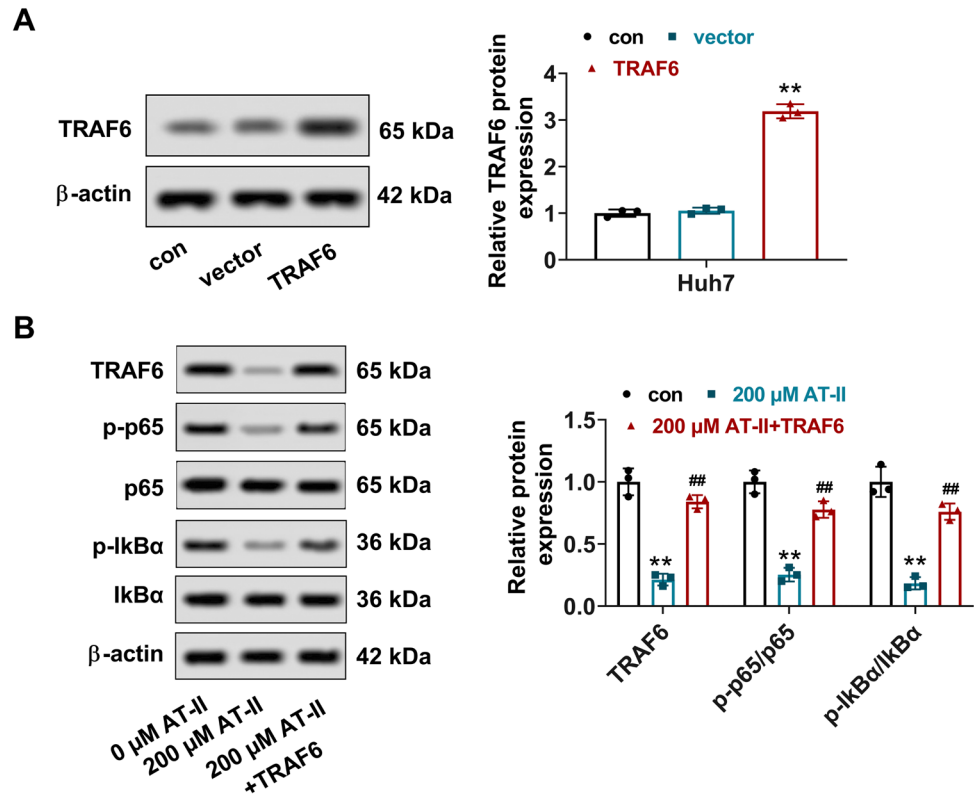


Fig. 5 Effect of AT-II on the expression of TRAF6/NF- κB pathway. Hep3B and Huh7 cells were treated with 50, 100, and 200 μM AT-II for 48 h. **A** and **B** The relative protein expression of TRAF6, p-p65, p-65, p-IkB α , and IkB α was examined by western blot. Data were

expressed after being normalized with β -actin. * $P < 0.05$ and ** $P < 0.01$ vs. 0 μM AT-II. **C** The level of p-65 was determined by IF after Hep3B and Huh7 cells were treated with 200 μM AT-II, and the cell nucleus was stained by DAPI. Scale bar = 25 μm . $n = 3$

Fig. 6 Overexpression of TRAF6 restored AT-II-induced reduction in the relative protein level of TRAF6, p-p65/p-65, and p-IkB α /IkB α in Huh7 cells. **A** The relative protein expression of TRAF6 was examined by western blot after Huh7 cells were transfected with pcDNA vector plasmids containing the sequences of TRAF6. Data were expressed after being normalized with β -actin. $**P < 0.01$ vs. vector. **B** The relative protein expression of TRAF6, p-p65, p-65, p-IkB α , and IkB α was examined by western blot. Data were expressed after being normalized with β -actin. $**P < 0.01$ vs. control; $##P < 0.01$ vs. 200 μ M AT-II. $n = 3$



tumor volume was supervised every 1 week for successive 4 weeks. Administration of AT-II observably declined tumor volume and weight, but had no influence on the mice body weight (Fig. 8A–D). Moreover, management of AT-II markedly decreased the level of GPX4, xCT, and PD-L1, while significantly elevated the CD8 level in tumor tissues (Fig. 8E and F). Furthermore, the introduction of AT-II prominently declined the relative protein level of TRAF6, p-p65/p-65, and p-IkB α /IkB α in tumor tissues (Fig. 8G). Hence, these results demonstrated that AT-II modulated the proliferation, ferroptosis, and immune escape involved in the downregulation of the TRAF6/NF- κ B pathway (Fig. 9).

Discussion

In the present study, AT-II inhibited proliferation and immune escape, but enhanced ferroptosis of both Hep3B and Huh7 cells. Mechanically, AT-II downregulated the expression of the TRAF6/NF- κ B pathway in both Hep3B and Huh7 cells, which was rescued with overexpression of TRAF6. Moreover, the upregulation of TRAF6 reversed the effect of AT-II on proliferation, ferroptosis, and immune escape in Hep3B cells. Furthermore, AT-II reduced tumor volume, tumor weight and the level of GPX4, xCT, and PD-L1 with the increased expression level of CD8. Besides, AT-II downregulated the expression of TRAF6/NF- κ B pathway *in vivo*.

Collectively, AT-II modulated the proliferation, ferroptosis, and immune escape of HCC cells by downregulating the TRAF6/NF- κ B pathway.

Sustaining proliferation is a fundamental and outstanding hallmark of all kinds of tumors, including hepatoma carcinoma (Hanahan 2022), thus agents that can inhibit tumor cell proliferation may be an alternative drug for tumor treatment. AT-II has exerted an anti-proliferative effect on a wide variety of tumor cells, including breast cell lines MDA-MB-231 and MCF-7 cells (Dou et al. 2021), colorectal cancer cell lines SW480 and Lovo cells (Zhang et al. 2019), prostate cancer cell lines DU145 and LNCaP cells (Wang et al. 2018), gastric carcinoma cell lines HGC-27 and AGS (Tian and Yu 2017), and melanoma cell lines B16 (Ye et al. 2011). Moreover, AT-II has been revealed to inhibit tumor growth in mice xenografted with melanoma (Fu et al. 2014). In line with these results, AT-II also declined the cell viability of both Hep3B and Huh7 cells, as well as tumor volume and weight in mice xenografted with Huh7 cells in the present study. Thus, AT-II suppressed tumor growth of HCC *in vitro* and *in vivo*.

Ferroptosis is a novel form of cell death, characterized by iron-elicited lipid peroxidation (Dixon et al. 2012). Glutathione peroxidase 4 (GPX4) and solute carrier family 7 member 11 (SLC7A11, also named xCT) are two crucial proteins related to ferroptosis. GPX4 belongs to the glutathione peroxidase family that can reduce toxic

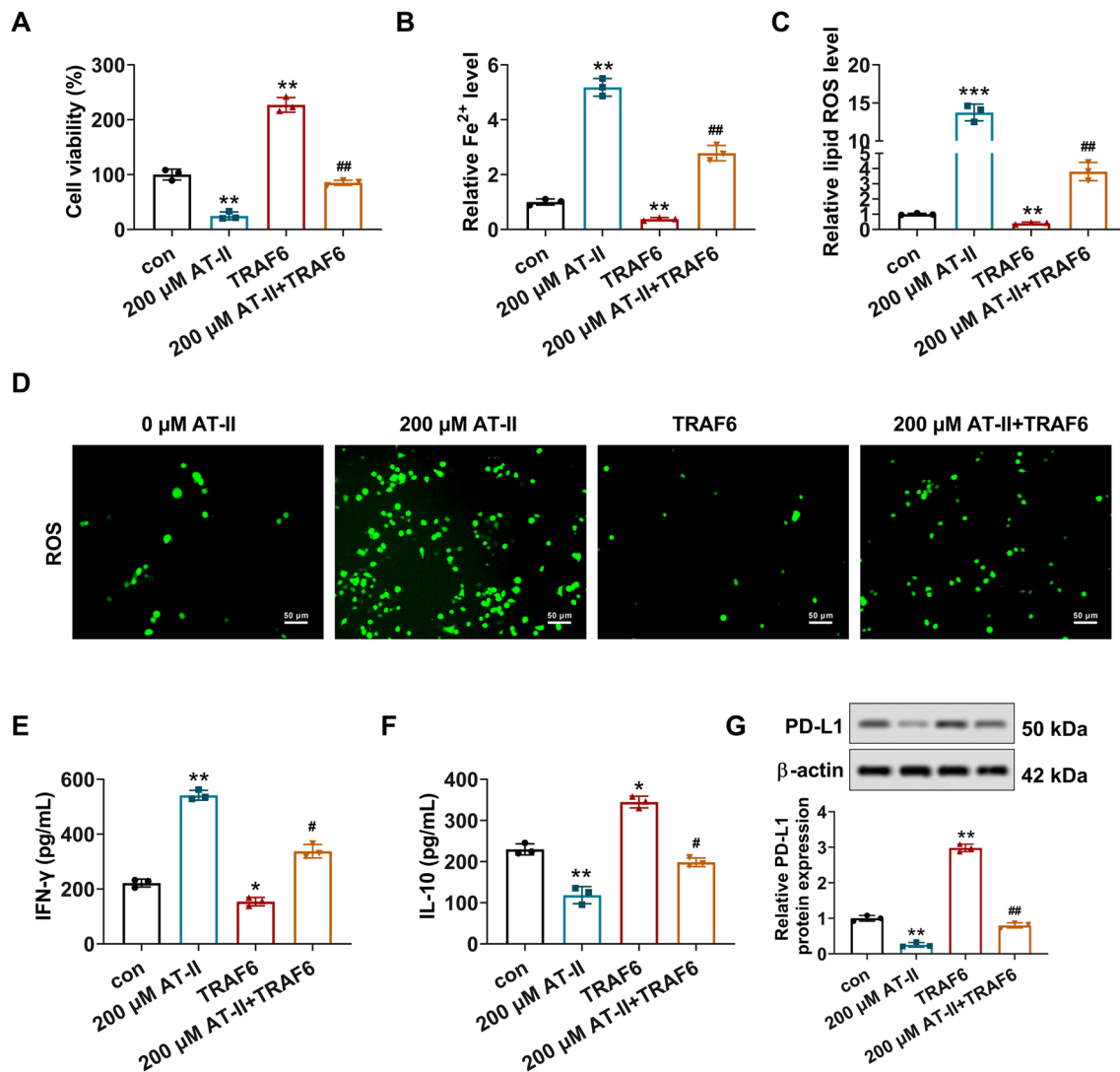


Fig. 7 AT-II modulated the proliferation, ferroptosis, and immune escape of Huh7 cells by inactivating the TRAF6/NF- κ B pathway. **A** The cell viability of Huh7 cells was detected by CCK-8. **B** Examination of the relative Fe²⁺ level in Huh7 cells. **C** and **D** Measurement of the relative ROS level in Huh7 cells. **E** The concentrations of IFN- γ

were measured by ELISA. **F** The concentrations of IL-10 were measured by ELISA. **G** The relative protein expression of PD-L1 was examined by western blot. Data were expressed after being normalized with β -actin. ** P < 0.01 and *** P < 0.001 vs. control; # P < 0.05 and ## P < 0.01 vs. 200 μ M AT-II. n = 3

phospholipid hydroperoxides to non-toxic phospholipid alcohols and astrict the generation of lipid peroxides (Fujii et al. 2020). xCT is an ingredient of the cystine/glutamate anti-porter that is primarily responsible for offering cysteine necessary for the synthesis of glutathione (GSH) (Dixon et al. 2012). Therefore, GPX4 and xCT are regarded as the key factors in preventing the occurrence of ferroptosis. Extensive reports have exhibited that ferroptosis is strongly related to the progression and development of hepatoma carcinoma. Ferroptosis is associated with the diagnosis, prognosis, and immunotherapy of hepatoma carcinoma (Ruan et al. 2023; Li et al. 2023). (Zi et al. 2023) identify uridine

as a potential target for hepatoma carcinoma therapy, in which uridine induces ferroptosis to suppress the development of hepatoma carcinoma. Lan and colleagues (Lan et al. 2023) show that saikosaponin A, the natural triterpenoid saponin from Radix Bupleuri, exerts an inhibitory effect on hepatoma carcinoma by enhancing ferroptosis. Moreover, AT-II has been revealed to decrease oxidative stress in mammary tumorigenesis (Wang et al. 2017). In the current study, AT-II increased the relative Fe²⁺ level, which was further promoted with the incubation of erastin and declined with the introduction of ferrostatin-1 in Hep3B and Huh7 cells. AT-II, however, declined the protein expression of GPX4

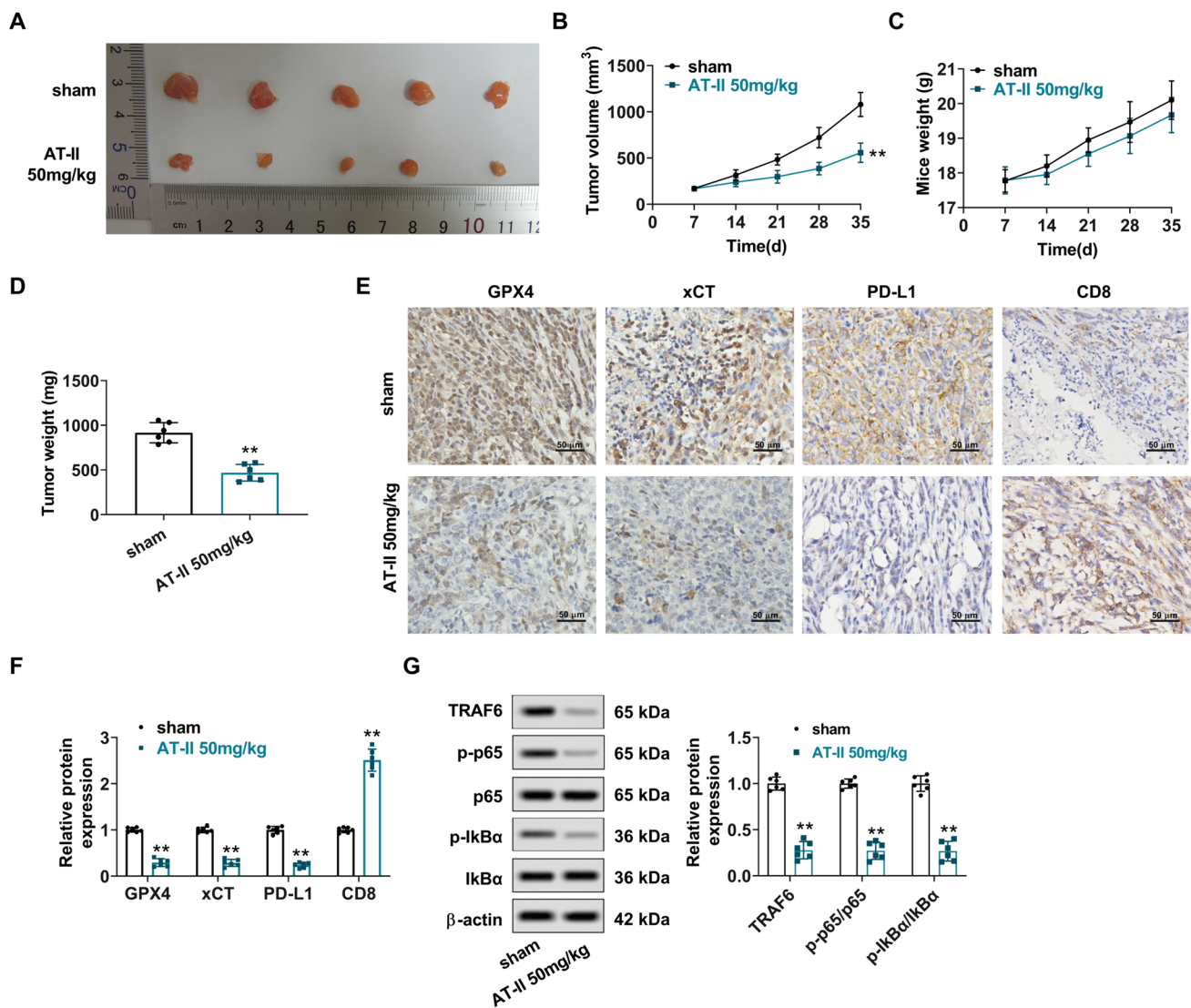


Fig. 8 AT-II modulated the proliferation, ferroptosis, and immune escape involved in the downregulation of the TRAF6/NF-κB pathway *in vivo*. **A** Representative image of neoplasms from nude mice. **B** Monitor of tumor volume every 1 week for successive 4 weeks. **C** Supervision of mouse body weight every 1 week for successive 4 weeks. **D** Measurement of tumor weight. **E** and **F** The expression lev-

els of GPX4, xCT, PD-L1, and CD8 in tumor tissues were detected by IHC. **G** The relative protein expression of TRAF6, p-p65, p-65, p-IκBα, and IκBα was determined by western blot. Results were expressed after being normalized with β-actin. ***P* < 0.01 vs. sham. *n* = 5

and xCT, which was rescued with the treatment of ferrostatin-1 in Hep3B and Huh7 cells. Besides, AT-II enhanced the level of ROS and MDA, but reduced the GSH level. Moreover, AT-II decreased the level of GPX4 and xCT in tumor tissues of xenografted mice. Thus, AT-II promoted ferroptosis in HCC.

Immune escape is another crucial cause of tumor occurrence (Hanahan 2022). Plenty of reports have exhibited that agents or targets inhibiting immune escape are potential

drugs or therapeutical targets for the treatment of HCC (Liang et al. 2023; Wang et al. 2023). In the present study, AT-II suppressed immune escape of HCC, as indicated by an increase in the percent of CD8+ T cells and the IFN-γ contents, and a decrease in the IL-10 concentrations and the expression of PD-L1 in Hep3B and Huh7 cells. Besides, AT-II declined the level of PD-L1, but upregulated the CD8 level in tumor tissues of xenografted mice. IFN-γ is a necessary cytokine that modulates immune

Liver cancer

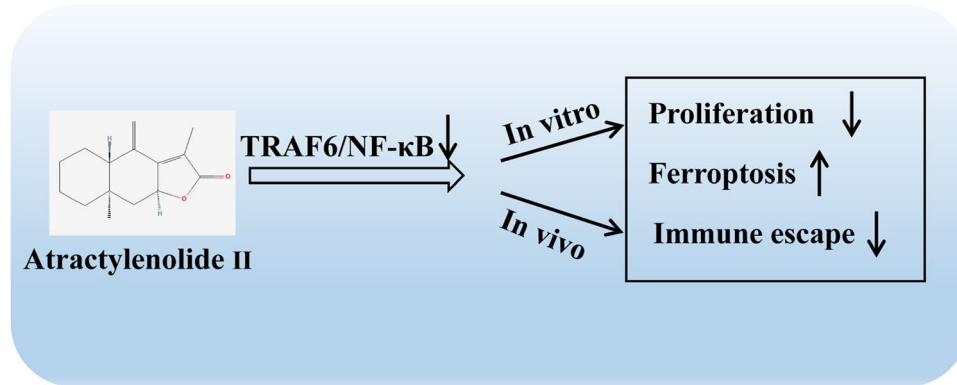


Fig. 9 Schematic diagram of the present study. AT-II inhibited proliferation and immune escape, but enhanced ferroptosis of HCC cells both *in vitro* and *in vivo*. Mechanically, AT-II downregulated the expression of TRAF6/NF- κ B pathway, and overexpression of TRAF6

reversed the effect of AT-II on proliferation, ferroptosis, and immune escape in HCC cells. Collectively, AT-II suppressed proliferation and immune escape, but promoted ferroptosis by downregulating the TRAF6/NF- κ B pathway in HCC

evasion related to the upregulation of immune checkpoint receptors, such as PD-L1 to vanish T cell activity in tumor tissues (Mulder et al. 2021; Liu et al. 2017). The overexpression of PD-L1 on tumor cells combined with the receptor PD-1 on T cells contributes to the immune escape through releasing negative modulatory signals, evoking T cell apoptosis or causing immune incompetence (Yi et al. 2022). Moreover, AT-II reduces inflammation in mammary tumorigenesis (Wang et al. 2017). Besides, several herbs that AT-II acts as the major ingredient have exhibited the inhibitory effect of inflammation, such as *Atractylodes lancea* (Hossen et al. 2021), *Atractylodes chinensis* (Hossen et al. 2019), and *Atractylodes japonica* Koidzumi (Chen et al. 2016). Therefore, AT-II suppressed immune escape in HCC.

TRAF6 is a member of the TRAF protein family that is crucial for modulating toll-like receptor (TLR)-mediated signaling (Akira et al. 2001). As the aggregated hub of signals elicited by tumor necrosis factor receptor and toll-like receptor families, TRAF6 mediates inflammatory and apoptotic signaling pathways to strongly participate in inflammatory and immune responses (Inoue et al. 2007). TRAF6 is a pivotal activator of NF- κ B signaling pathway by binding to NF- κ B-evoked kinase and other signaling molecules (Ye et al. 2002). Prominently, TRAF6 regulates the NF- κ B signaling pathway that plays a vital role in tumorigenesis. High expression of TRAF6 in colorectal cancer forecasts poor survival in patients, and activates the TRAF6/NF- κ B signaling pathway to exacerbate colorectal cancer (Zhu et al. 2019). The promoted role of GTPase M in M2 phenotype macrophage polarization is mediated by the TRAF6/NF- κ B pathway, which expedites the progression of gliomas (Xu et al. 2019). Downregulation in TRAF6/NF- κ B signaling

is revealed to be involved in the accelerative effect of gold nanoparticles on radiosensitivity in glioma (Wang et al. 2023). Asiaticoside inhibits the activity of TRAF6/NF- κ B to slow down the osteosarcoma progression (Li and Wang 2022). Notoginsenoside R1 suppresses cell proliferation and enhances oxidative stress through the inactivation of TRAF6/NF- κ B signaling in nasopharyngeal carcinoma (Li et al. 2022). Moreover, TRAF6/NF- κ B signaling has been exhibited to be tightly relevant to the development of HCC (Wan et al. 2018; Hu et al. 2020). Moreover, AT-II has been revealed to be closely related to the regulation of NF- κ B signaling in various diseases, such as rheumatoid arthritis (Gao et al. 2023), and gastritis (Hossen et al. 2019). Here, AT-II attenuated the expression of TRAF6/NF- κ B in HCC both *in vitro* and *in vivo*. Furthermore, overexpression of TRAF6 also reversed the effect of AT-II on proliferation, ferroptosis, and immune escape in Hep3B cells. Altogether, AT-II regulated the proliferation, ferroptosis, and immune escape of HCC cells by inactivating the TRAF6/NF- κ B pathway.

In summary, AT-II inhibited proliferation and immune escape, but enhanced ferroptosis by downregulating the TRAF6/NF- κ B pathway in HCC. The results provide a better understanding and the potential selection for the drugs of the HCC treatment. However, several limitations should be addressed in the following study. Firstly, the effect of AT-II on other signaling pathways, such as MAPKp38/Nrf2, JAK2/STAT3, and Akt/ERK, can be investigated *in vivo*. Secondly, the effect of AT-II on the other malignant processes, such as invasion, epithelial-mesenchymal transition (EMT), metabolism, and stemness, can be surveyed in the subsequent assays.

Authors contributions LJ and PZ conceived and designed research. LJ, SW and ZM conducted experiments. CK contributed new reagents or analytical tools. LJ and WY analyzed data. LJ wrote the manuscript. All authors read and approved the manuscript. The authors declare that all data were generated in-house and that no paper mill was used.

Funding We received support from the Guangdong Provincial Bureau of Traditional Chinese Medicine under Grant 20231056; Basic and Applied Basic Research Foundation of Guangdong Province, Provincial Enterprise Joint Fund (2023A1515220248).

Data availability The datasets used and/or analyzed during the present study are available from the corresponding author on reasonable request.

Declarations

Competing interests The authors declare no competing interests.

References

- Akira S, Takeda K, Kaisho T (2001) Toll-like receptors: critical proteins linking innate and acquired immunity. *Nat Immunol* 2:675–680. <https://doi.org/10.1038/90609>
- Bray F, Ferlay J, Soerjomataram I et al (2018) Global cancer statistics 2018: GLOBOCAN estimates of incidence and mortality worldwide for 36 cancers in 185 countries. *CA Cancer J Clin* 68:394–424. <https://doi.org/10.3322/caac.21492>
- Cai LY, Chen SJ, Xiao SH et al (2021) Targeting p300/CBP attenuates hepatocellular carcinoma progression through epigenetic regulation of metabolism. *Cancer Res* 81:860–872. <https://doi.org/10.1158/0008-5472.Can-20-1323>
- Cardenas M, Blank VC, Zotta E et al (2009) Induction of apoptosis in vitro and in vivo effects of a synthetic nitroflavone derivative on murine mammary adenocarcinoma cells. *Cancer Res* 69:2145
- Chen LG, Jan YS, Tsai PW et al (2016) Anti-inflammatory and antinociceptive constituents of *Atractylodes japonica* Koidzumi. *J Agric Food Chem* 64:2254–2262. <https://doi.org/10.1021/acs.jafc.5b05841>
- Chen W, Chiang CL, Dawson LA (2021) Efficacy and safety of radiotherapy for primary liver cancer. *Chin Clin Oncol* 10:9. <https://doi.org/10.21037/cco-20-89>
- Dixon SJ, Lemberg KM, Lamprecht MR et al (2012) Ferroptosis: an iron-dependent form of nonapoptotic cell death. *Cell* 149:1060–1072. <https://doi.org/10.1016/j.cell.2012.03.042>
- Dou S, Yang C, Zou D et al (2021) Atractylenolide II induces cell cycle arrest and apoptosis in breast cancer cells through ER pathway. *Pak J Pharm Sci* 34:1449–1458
- Fu XQ, Chou GX, Kwan HY et al (2014) Inhibition of STAT3 signaling contributes to the antimelanoma action of atractylenolide II. *Exp Dermatol* 23:855–857. <https://doi.org/10.1111/exd.12527>
- Fujii J, Homma T, Kobayashi S (2020) Ferroptosis caused by cysteine insufficiency and oxidative insult. *Free Radic Res* 54:969–980. <https://doi.org/10.1080/10715762.2019.1666983>
- Galle PR, Dufour JF, Peck-Radosavljevic M et al (2021) Systemic therapy of advanced hepatocellular carcinoma. *Future Oncol* 17:1237–1251. <https://doi.org/10.2217/fon-2020-0758>
- Gao Y, Xin D, Liang XD et al (2023) Effect of a combination of *Atractylodes macrocephala* extract with strychnine on the TLR4/NF- κ B/NLRP3 pathway in MH7A cells. *Exp Ther Med* 25:91. <https://doi.org/10.3892/etm.2023.11791>
- Hanahan D (2022) Hallmarks of cancer: new dimensions. *Cancer Discov* 12:31–46. <https://doi.org/10.1158/2159-8290.Cd-21-1059>
- Hossen MJ, Chou JY, Li SM et al (2019) An ethanol extract of the rhizome of *Atractylodes chinensis* exerts anti-gastritis activities and inhibits Akt/NF- κ B signaling. *J Ethnopharmacol* 228:18–25. <https://doi.org/10.1016/j.jep.2018.09.015>
- Hossen MJ, Amin A, Fu XQ et al (2021) The anti-inflammatory effects of an ethanolic extract of the rhizome of *Atractylodes lancea*, involves Akt/NF- κ B signaling pathway inhibition. *J Ethnopharmacol* 277:114183. <https://doi.org/10.1016/j.jep.2021.114183>
- Hu YL, Feng Y, Chen YY et al (2020) SNHG16/miR-605-3p/TRAF6/NF- κ B feedback loop regulates hepatocellular carcinoma metastasis. *J Cell Mol Med* 24:7637–7651. <https://doi.org/10.1111/jcmm.15399>
- Inoue J, Gohda J, Akiyama T (2007) Characteristics and biological functions of TRAF6. *Adv Exp Med Biol* 597:72–79. https://doi.org/10.1007/978-0-387-70630-6_6
- Kishore SA, Bajwa R, Madoff DC (2020) Embolotherapeutic strategies for hepatocellular carcinoma: 2020 update. *Cancers (Basel)* 12:791. <https://doi.org/10.3390/cancers12040791>
- Konyn P, Ahmed A, Kim D (2021) Current epidemiology in hepatocellular carcinoma. *Expert Rev Gastroenterol Hepatol* 15:1295–1307. <https://doi.org/10.1080/17474124.2021.1991792>
- Lan T, Wang W, Zeng XX et al (2023) Saikosaponin A triggers cell ferroptosis in hepatocellular carcinoma by inducing endoplasmic reticulum stress-stimulated ATF3 expression. *Biochem Biophys Res Commun* 674:10–18. <https://doi.org/10.1016/j.bbrc.2023.06.086>
- Li DK, Wang GH (2022) Asiaticoside reverses M2 phenotype macrophage polarization-evoked osteosarcoma cell malignant behaviour by TRAF6/NF- κ B inhibition. *Pharm Biol* 60:1635–1645. <https://doi.org/10.1080/13880209.2022.2109688>
- Li CQ, He LC, Jin JQ (2007) Atractylenolide I and atractylenolide III inhibit Lipopolysaccharide-induced TNF- α and NO production in macrophages. *Phytother Res* 21:347–353. <https://doi.org/10.1002/ptr.2040>
- Li CQ, He LC, Dong HY et al (2007) Screening for the anti-inflammatory activity of fractions and compounds from *Atractylodes macrocephala* koidz. *J Ethnopharmacol* 114:212–217. <https://doi.org/10.1016/j.jep.2007.08.002>
- Li S, Pi G, Zeng Y et al (2022) Notoginsenoside R1 induces oxidative stress and modulates LPS induced immune microenvironment of nasopharyngeal carcinoma. *Int Immunopharmacol* 113:109323. <https://doi.org/10.1016/j.intimp.2022.109323>
- Li C, Cui X, Li Y et al (2023) Identification of ferroptosis and drug resistance related hub genes to predict the prognosis in Hepatocellular Carcinoma. *Sci Rep* 13:8681. <https://doi.org/10.1038/s41598-023-35796-z>
- Liang X, Gao H, Xiao J et al (2023) Abrine, an IDO1 inhibitor, suppresses the immune escape and enhances the immunotherapy of anti-PD-1 antibody in hepatocellular carcinoma. *Front Immunol* 14:1185985. <https://doi.org/10.3389/fimmu.2023.1185985>
- Liu Y, Liang X, Yin X et al (2017) Blockade of IDO-kynurenine-AhR metabolic circuitry abrogates IFN- γ -induced immunologic dormancy of tumor-repopulating cells. *Nat Commun* 8:15207. <https://doi.org/10.1038/ncomms15207>
- Mulder K, Patel AA, Kong WT et al (2021) Cross-tissue single-cell landscape of human monocytes and macrophages in health and disease. *Immunity* 54:1883–1900.e1885. <https://doi.org/10.1016/j.immuni.2021.07.007>
- Nia A, Dhanasekaran R (2020) Genomic landscape of HCC. *Curr Hepatol Rep* 19:448–461. <https://doi.org/10.1007/s11901-020-00553-7>
- Ruan WY, Zhang L, Lei S et al (2023) An inflammation-associated ferroptosis signature optimizes the diagnosis, prognosis evaluation and immunotherapy options in hepatocellular carcinoma. *J Cell Mol Med*. <https://doi.org/10.1111/jcmm.17780>
- Sheng L, Li J, Li N et al (2021) Atractylenolide III predisposes miR-195-5p/FGFR1 signaling axis to exert tumor-suppressive

- functions in liver cancer. *J Food Biochem* 45:e13582. <https://doi.org/10.1111/jfbc.13582>
- Sugawara Y, Hibi T (2021) Surgical treatment of hepatocellular carcinoma. *Biosci Trends* 15:138–141. <https://doi.org/10.5582/bst.2021.01094>
- Tian S, Yu H (2017) Atractylenolide II inhibits proliferation, motility and induces apoptosis in human gastric carcinoma cell lines HGC-27 and AGS. *Molecules* 22:1886. <https://doi.org/10.3390/molecules22111886>
- Vogel A, Meyer T, Sapisochin G et al (2022) Hepatocellular carcinoma. *Lancet* 400:1345–1362. [https://doi.org/10.1016/s0140-6736\(22\)01200-4](https://doi.org/10.1016/s0140-6736(22)01200-4)
- Wan C, Wu M, Zhang S et al (2018) $\alpha 7$ nAChR-mediated recruitment of PP1 γ promotes TRAF6/NF- κ B cascade to facilitate the progression of Hepatocellular Carcinoma. *Mol Carcinog* 57:1626–1639. <https://doi.org/10.1002/mc.22885>
- Wang KT, Chen LG, Wu CH et al (2010) Gastroprotective activity of atractylenolide III from *Atractylodes ovata* on ethanol-induced gastric ulcer in vitro and in vivo. *J Pharm Pharmacol* 62:381–388. <https://doi.org/10.1211/jpp.62.03.0014>
- Wang KT, Chen LG, Chou DS et al (2011) Anti-oxidative abilities of essential oils from *Atractylodes ovata* rhizome. *Evid Based Complement Alternat Med* 2011:204892. <https://doi.org/10.1093/ecam/nea006>
- Wang T, Long F, Zhang X et al (2017) Chemopreventive effects of atractylenolide II on mammary tumorigenesis via activating Nrf2-ARE pathway. *Oncotarget* 8:77500–77514. <https://doi.org/10.18632/oncotarget.20546>
- Wang J, Nasser MI, Adlat S et al (2018) Atractylenolide II induces apoptosis of prostate cancer cells through regulation of AR and JAK2/STAT3 signaling pathways. *Molecules* 23:3297. <https://doi.org/10.3390/molecules23123298>
- Wang H, Xu Q, Dong X et al (2023) Gold nanoparticles enhances radiosensitivity in glioma cells by inhibiting TRAF6/NF- κ B induced CCL2 expression. *Heliyon* 9:e14362. <https://doi.org/10.1016/j.heliyon.2023.e14362>
- Wang H, Tang A, Cui Y et al (2023) LRPPRC facilitates tumor progression and immune evasion through upregulation of m6A modification of PD-L1 mRNA in hepatocellular carcinoma. *Front Immunol* 14:1144774. <https://doi.org/10.3389/fimmu.2023.1144774>
- Xiao C, Xu C, He N et al (2020) Atractylenolide II prevents radiation damage via MAPKp38/Nrf2 signaling pathway. *Biochem Pharmacol* 177:114007. <https://doi.org/10.1016/j.bcp.2020.114007>
- Xie Z, Lin M, He X et al (2023) Chemical constitution, pharmacological effects and the underlying mechanism of atractylenolides: a review. *Molecules* 28:3987. <https://doi.org/10.3390/molecules28103987>
- Xu Y, Liao C, Liu R et al (2019) IRGM promotes glioma M2 macrophage polarization through p62/TRAF6/NF- κ B pathway mediated IL-8 production. *Cell Biol Int* 43:125–135. <https://doi.org/10.1002/cbin.11061>
- Ye H, Arron JR, Lamothe B et al (2002) Distinct molecular mechanism for initiating TRAF6 signalling. *Nature* 418:443–447. <https://doi.org/10.1038/nature00888>
- Ye Y, Wang H, Chu JH et al (2011) Atractylenolide II induces G1 cell-cycle arrest and apoptosis in B16 melanoma cells. *J Ethnopharmacol* 136:279–282. <https://doi.org/10.1016/j.jep.2011.04.020>
- Yi M, Zheng X, Niu M et al (2022) Combination strategies with PD-1/PD-L1 blockade: current advances and future directions. *Mol Cancer* 21:28. <https://doi.org/10.1186/s12943-021-01489-2>
- Zhang R, Wang Z, Yu Q et al (2019) Atractylenolide II reverses the influence of lncRNA XIST/miR-30a-5p/ROR1 axis on chemoresistance of colorectal cancer cells. *J Cell Mol Med* 23:3151–3165. <https://doi.org/10.1111/jcmm.14148>
- Zhang H, Ge Z, Wang Z et al (2021) Circular RNA RHOT1 promotes progression and inhibits ferroptosis via mir-106a-5p/STAT3 axis in breast cancer. *Aging (Albany NY)* 13:8115–8126. <https://doi.org/10.18632/aging.202608>
- Zhang Y, Liu Y, Wang J et al (2022) Atractylenolide II inhibits tumor-associated macrophages (TAMs)-induced lung cancer cell metastasis. *Immunopharm Immunotoxicol* 44:227–237. <https://doi.org/10.1080/08923973.2022.2037629>
- Zhou H, Song T (2021) Conversion therapy and maintenance therapy for primary hepatocellular carcinoma. *Biosci Trends* 15:155–160. <https://doi.org/10.5582/bst.2021.01091>
- Zhu G, Cheng Z, Huang Y et al (2019) TRAF6 promotes the progression and growth of colorectal cancer through nuclear shuttle regulation NF- κ B/c-jun signaling pathway. *Life Sci* 235:116831. <https://doi.org/10.1016/j.lfs.2019.116831>
- Zi L, Ma W, Zhang L et al (2023) Uridine inhibits hepatocellular carcinoma cell development by inducing ferroptosis. *J Clin Med* 12:3552. <https://doi.org/10.3390/jcm12103552>

Publisher's Note Springer Nature remains neutral with regard to jurisdictional claims in published maps and institutional affiliations.

Springer Nature or its licensor (e.g. a society or other partner) holds exclusive rights to this article under a publishing agreement with the author(s) or other rightsholder(s); author self-archiving of the accepted manuscript version of this article is solely governed by the terms of such publishing agreement and applicable law.